EXPERT VIEW

Microsensors in plant biology: *in vivo* visualization of inorganic analytes with high spatial and/or temporal resolution

Ole Pedersen[1,2,*], Niels Peter Revsbech[3] and Sergey Shabala[4,5]

[1] Department of Biology, University of Copenhagen, Denmark
[2] School of Agriculture and Environment, The University of Western Australia, Australia
[3] Aarhus University Centre for Water Technology, Department of Bioscience, Aarhus University, Denmark
[4] School of Land and Food, University of Tasmania, Australia
[5] International Research Centre for Environmental Membrane Biology, Foshan University, China

* Correspondence: opedersen@bio.ku.dk

Editor: Richard Napier, University of Warwick, UK

Abstract

This Expert View provides an update on the recent development of new microsensors, and briefly summarizes some novel applications of existing microsensors, in plant biology research. Two major topics are covered: (i) sensors for gaseous analytes (O_2, CO_2, and H_2S); and (ii) those for measuring concentrations and fluxes of ions (macro- and micronutrients and environmental pollutants such as heavy metals). We show that application of such microsensors may significantly advance understanding of mechanisms of plant–environmental interaction and regulation of plant developmental and adaptive responses under adverse environmental conditions via non-destructive visualization of key analytes with high spatial and/or temporal resolution. Examples included cover a broad range of environmental situations including hypoxia, salinity, and heavy metal toxicity. We highlight the power of combining microsensor technology with other advanced biophysical (patch–clamp, voltage–clamp, and single-cell pressure probe), imaging (MRI and fluorescent dyes), and genetic techniques and approaches. We conclude that future progress in the field may be achieved by applying existing microsensors for important signalling molecules such as NO and H_2O_2, by improving selectivity of existing microsensors for some key analytes (e.g. Na, Mg, and Zn), and by developing new microsensors for P.

Keywords: Ion flux, microelectrode, micro-optode, MIFE, tissue CO_2, tissue O_2.

Introduction

Microsensors are useful tools in many areas of plant biology where they are utilized to measure concentration profiles of various gaseous or ionic analytes and the kinetics of their changes. Microsensors are also widely used to study kinetics of fluxes of analytes between tissues and the environment. In both cases, the measurements are considered as non–destructive. The small size of the microsensors and their fast response time make them highly powerful tools to study temporal concentration changes of the analyte in question, or its flux from the specific tissue. Such techniques can also be used to 'map' ion or gas profiles around the plant tissue. This Expert View provides an update on the recent development of new microsensors,

and briefly summarizes some novel applications of existing microsensors. We hope that such information might inspire new research lines and assist in addressing some long-standing questions in the field of plant biology.

Microsensors have high spatial resolution due to the small tip size. As a rule of thumb, the spatial resolution of a microsensor is equal to the diameter of the tip. This is mainly due to physical impact considerations since microsensors with larger and reinforced tips can be constructed to have the same low consumption rate of the analyte but the physical impact on the plant tissue is considerably higher. At present, the smallest Clark-type O_2 microsensors have tip diameters of ~3 µm (Table 1) meaning that gradients in O_2 can be resolved not only at the tissue level (Weits *et al.*, 2019) but also to some extent at the cell level. This is also true for ion-selective microelectrodes that typically have a tip diameter of 3–4 µm and thus allow the kinetics of ion exchange from the single cell (Tegg *et al.*, 2005) or isolated cellular organelles to be quantified (Pottosin *et al.*, 2009).

Generally, microsensors exhibit fast responds to concentration changes in analytes compared with their macrosensor counterparts. Fast diffusional equilibration of concentration gradients around the sensor tip is the main reason for the rapid responses. For Clark-type gas sensors, the tiny membrane separating the sensor interior from the environment and the close proximity of internal electrodes to the membrane are essential for the fast response. Clark-type O_2 microsensors can be made with a response time of <200 ms, for example enabling layer-specific measurement of photosynthetic rates in millimetre thick microbial mats (Lassen *et al.*, 1998). Most ion-selective microelectrodes using liquid ionophores [liquid ion exchangers (LIXs)] have similarly fast response times.

Here we restrict our focus to microsensors for inorganic analytes since microsensors for organic compounds, including phytohormones, have recently been reviewed (Sadanandom and Napier, 2010; Walia *et al.*, 2018). Microsensors for inorganic compounds may be divided into (i) gaseous analytes with emphasis on O_2 and CO_2; and (ii) ionic analytes mainly to quantify fluxes of essential macro- and micronutrients and environmental pollutants (e.g. heavy metals) between plant tissues and the environment using microelectrode ion flux measurements (the MIFE technique), with the key developments presented in Box 1. We use the term 'microsensor' whenever the sensor is combined into a single unit. This is the case for an amperometric sensor where the anode and cathode are fused into one sensor or for a voltametric sensor where the reference and measuring electrode are combined into a single unit. The term 'electrode' is used when an external 'reference' is needed. In addition to the microsensors covered by this Expert View, other microsensors are available, some of which could be of potential use in plant biology. Examples include a spherical light sensor with a typical diameter of the light-sensing sphere of only 70 µm (Lassen *et al.*, 1992), but the N_2O (Andersen *et al.*, 2001) or CH_4 (Damgaard and Revsbech, 1997) microsensors, both with tip diameters down to 20 µm, might also be of interest to plant biologists. Interestingly, the NO or H_2O_2 microsensor has not yet been introduced in plant biology (see

Table 1. Selected examples of recent application of microsensors and microelectrodes for various gaseous or ionic analytes in plant biology

Analytes	Electrode type/tip size/technique	Examples of recent application in plant biology
Oxygen (O_2)	0.1–0.5 µm (carbon fibre) 1–100 µm (Clark-type) 50–500 µm (glass fibre)	O_2 dynamics in plant tissues (Mori *et al.*, 2019; Weits *et al.*, 2019; Alova *et al.*, 2020; Brodersen *et al.*, 2020; Pedersen *et al.*, 2020)
Carbon dioxide (CO_2)	30–50 µm	Tissue CO_2 dynamics and CO_2 fluxes (Pedersen *et al.*, 2018; Brodersen *et al.*, 2020; Colmer *et al.*, 2020)
Hydrogen sulfide (H_2S)	10–100 µm	H_2S intrusion in seagrasses (Brodersen et al., 2017, 2018; Johnson *et al.*, 2018)
Nitric oxide (NO)	15–100 µm	See Meng *et al.* (2017) for an example in medicine
Hydrogen peroxide (H_2O_2)	10 µm	See Kulagina and Michael (2003) for an example in medicine or Koren *et al.* (2016) for an example in microbiology
Nitrate (NO_3^-)	NMT technique	Sa *et al.* (2019) influence of ectomycorrhiza; Tang *et al.* (2019) interaction between NO_3^- and NH_4^+
Ammonium (NH_4^+)	NMT technique	Effects of brassinosteriods (Anwar *et al.*, 2019); effects of Si (Sheng *et al.*, 2018)
Potassium (K^+)	MIFE technique	Hypoxia tolerance (Gill *et al.*, 2018); ROS regulation (Wang *et al.*, 2018); nanoparticles (Wu *et al.*, 2018)
Sodium (Na^+)	MIFE technique NMT technique	Screening for SOS1 activity (Wu *et al.*, 2019); salinity tolerance in rice (Liu *et al.*, 2019); effects of ATP (Zhao *et al.*, 2016)
Calcium (Ca^{2+})	NMT technique MIFE technique	Effect of B (Zhou *et al.*, 2017); salt tolerance in cereals (Wang *et al.*, 2018)
Hydrogen (H^+)	MIFE technique	Effect of GABA (Su *et al.*, 2019); salinity tolerance in Cucurbitaceae (Huang *et al.*, 2019); B and Al toxicity (Li *et al.*, 2018)
Cadmium (Cd^{2+})	NMT technique	Interaction between Zn and Cd (Wu *et al.*, 2019); hyperaccumulators (Zhang *et al.*, 2016)
Lead (Pb^{2+})	NMT technique	Effects of NO (Wu *et al.*, 2019)

Box 1. Key developments in microsensors for the plant biologists

- **Oxygen (O$_2$)** Molecular O$_2$ can be measured with amperometric or optical microsensors. A current application of the world's smallest Clark-type O$_2$ sensor with a tip diameter of only 3 µm revealed the existence of stem cells enveloped in a hypoxic niche of the shoot apical meristem of Arabidopsis (Weits *et al.*, 2019); see Box 3.
- **Carbon dioxide (CO$_2$)** A novel amperometric CO$_2$ microsensor with a tip diameter of 35 µm has recently been used to 'unlock the doors to a secret chamber' inside roots and leaves of plants. The CO$_2$ microsensor enabled acquisition of tissue CO$_2$ dynamics in leaves of C$_3$ and CAM plants (Pedersen *et al.*, 2018) or tissue-specific CO$_2$ concentrations in waterlogged roots (Colmer *et al.*, 2020); see Box 2.
- **Sulfide (H$_2$S)** A H$_2$S microsensors with a tip diameter of 25 µm was used under challenging field conditions to demonstrate intrusion of toxic H$_2$S into belowground tissues of a seagrass (Brodersen *et al.*, 2017). In the laboratory, measurements of tissue H$_2$S dynamics have revealed key environmental conditions resulting in H$_2$S intrusion (Johnson *et al.*, 2018).
- **Nitric oxide (NO)** NO plays a key role in a number of signalling processes during abiotic stress responses in plants (Yu *et al.*, 2014). However, even if the NO microsensor (tip diameter down to 15 µm) is commercially available, it has not yet been applied to plant tissues.
- **Essential macro- (K, Ca, Mg, NH$_4$, NO$_3$, and SO$_4$) and micro- (Cu, Zn, Cl, and Ni) nutrients** Commercial liquid ion exchangers (LIXs) are available for these nutrients as well as some other ions of interest (H$^+$, Na$^+$, Cd^{2+}, Pb^{2+}, and Li$^+$). Microelectrodes are prepared on a daily basis and have a shelf-life of 10–12 h without any significant changes in their characteristics. The electrode tip diameter is typically 2–3 µm, and net ion fluxes can be measured by the MIFE system with high temporal (~5 s) resolution from a broad range of plant systems—from root (e.g. epidermis, cortex, or stele) and leaf (mesophyll or epidermis) tissues to single cells (e.g. stomatal guard cell, pollen tube, or root hair) and isolated organelles (vacuoles or chloroplasts). Thus, the MIFE technique represents a powerful tool for revealing and quantifying the role of specific ion transporters in plant adaptive responses to salinity, waterlogging, osmotic stress, chilling, acidity, elicitors, and oxidative stress, as well as to understand the signalling cascades mediating plant–environment interactions.
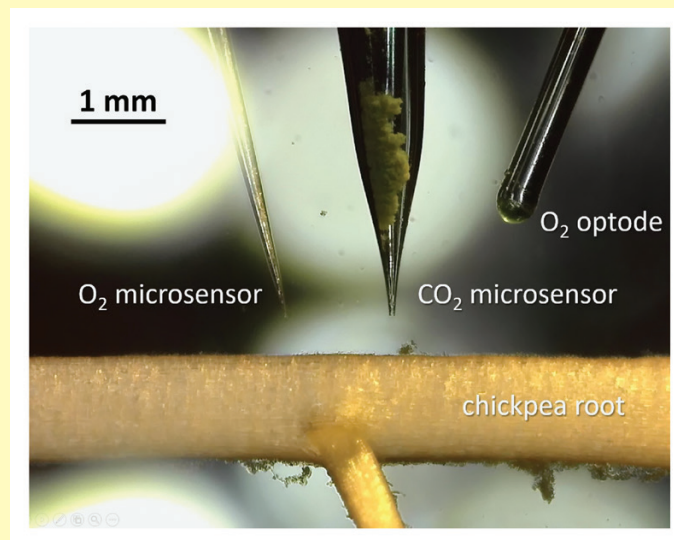
The novel CO$_2$ microsensor, a conventional O$_2$ microsensor, and an O$_2$ optode hover above the root of a chickpea seedling. The two microsensors can be moved simultaneously to obtain discrete measurements of O$_2$ and CO$_2$ in the diffusive boundary layer enveloping the root. These measurements are subsequently used to calculate fluxes of O$_2$ (consumption) and CO$_2$ (production) between the medium and root tissues (see text).

Table 1) although both analytes serve as important regulatory or signalling molecules (Slesak *et al.*, 2007; Wany *et al.*, 2017).

Gaseous analytes (O$_2$, CO$_2$, and H$_2$S)

Oxygen (O$_2$)

Most O$_2$ microsensors are miniaturized Clark-type sensors (Clark, 1956). At air equilibrium, a typical signal from a Clark-type O$_2$ microsensor is 100 pA. Thus, this type of O$_2$ microsensor consumes a very insignificant amount of O$_2$; it would take 35 years for such a sensor to consume all O$_2$ present in 1 ml of water initially at air equilibrium at 25 °C (Gundersen *et al.*, 1998). Nevertheless, the fact that there is some oxygen consumption by the sensor also makes the Clark-type microsensors slightly sensitive to stirring (between 1% and 3% for a typical microsensor; Revsbech, 1989). This sensitivity is a function of the response time; the faster the response time, the higher the stirring sensitivity.

In contrast to the Clark-type O$_2$ microsensor, the O$_2$ micro-optode is neither sensitive to stirring, nor does it consume O$_2$ (Klimant *et al.*, 1997). The O$_2$ micro-optode is likewise a miniaturized version of its macro counterpart where a fibre glass is coated with luminophores that emit light when excited with either red or blue light. The emitted light is, however, quenched in the presence of O$_2$ in a characteristic way so that the O$_2$ concentration can be determined. Optode-based microsensors for O$_2$ are particularly sensitive at low O$_2$ concentrations since the signal of the sensor increases with declining O$_2$ concentrations, and, by selection of suitable luminophores and polymers, the detection limit may be brought down into the low nanomolar range (Lehner *et al.*, 2015). It should, however, be kept in mind that an O$_2$ micro-optode does not respond as fast as a Clark-type O$_2$ microsensor and a wide range of compounds (mainly organic) can interfere with the signal. For a plant biologist, the main disadvantage is the flexible nature of the fibre that makes is difficult to penetrate plant tissues. This is not an issue with the Clark-type sensors where the tips can be made very small (e.g. 3–5 μm, Table 1), and the stiffness of the glass capillaries makes the sensors particularly suitable for penetrating plant tissues.

A carbon fibre-based O$_2$ nanoelectrode is an exciting development in the attempt to make the O$_2$ sensor even smaller (Alova *et al.*, 2020). The tip size is an order of magnitude smaller than that of the smallest Clark-type sensors (Weits *et al.*, 2019) but the carbon fibre electrode needs further technical development in order to demonstrate its potential for extremely high spatial resolution. So far, its application has been limited to time series with relatively poor time resolution (6 s; Alova *et al.* (2020); the best Clark-type O$_2$ microsensor would have 90% response times of <200 ms (Lassen *et al.*, 1997).

Recent applications of O$_2$ microsensors in plant biology

A custom-built Clark-type O$_2$ microsensor was recently used to reveal a hypoxic niche inside the shoot apical meristem of Arabidopsis (Weits *et al.*, 2019); see Box 2. The tip of the sensor was only 3 μm, enabling insertion into 4-day-old seedlings.

High resolution tissue O$_2$ profiles in roots of chickpea were also obtained by a Clark-type O$_2$ microsensor, revealing the expansion of an anoxic core as the external O$_2$ supply declined (Colmer *et al.*, 2020); see Box 2. The substantial drop in O$_2$ tissue status inside the vascular cylinder is caused by a combination of a low tissue porosity resulting in low diffusivity and a higher O$_2$ demand inside the vascular cylinder as compared with the surrounding porous cortex (figure in Box 3). Until now, only a small number of studies used radial O$_2$ profiles in plant roots, and the emphasis has been on monocots (Armstrong *et al.*, 2019).

Recently, micro-optodes have been used to study O$_2$ dynamics in the stem of deepwater rice (Mori *et al.*, 2019) and the shoot meristem of seagrasses (Pedersen *et al.*, 2016). Optodes do not require calibration as often as Clark-type sensors and are thus particularly useful for studies involving diurnal time series of tissue O$_2$ dynamics. In both studies, the glass fibre was embedded in a hypodermic needle to enable insertion of the flexible glass fibre into the tissues; this allowed measurements to be carried out under challenging field conditions. The deployment of the O$_2$ micro-optodes in seagrasses lasted for up to 24 h and revealed that anoxia during night-time was replaced with periods of hyperoxia only 9 h later with up to 50 kPa pO$_2$ inside the basal part of the shoot meristem (Pedersen *et al.*, 2016). In experiments with deepwater rice, continuous O$_2$ measurements lasted even longer (up to 72 h; thanks to the long-term stability of the O$_2$ optode and its excellent temperature compensation) and showed that the diurnal amplitude in tissue O$_2$ was substantially higher in completely submerged plants compared with those that were partially submerged (Mori *et al.*, 2019). Completely submerged plants were severely hypoxic during the night-time but experienced hyperoxic conditions during the day, with the tissue pO$_2$ up to 35 kPa.

Carbon dioxide (CO$_2$)

CO$_2$ microsensors of the Severinghaus-type (Severinghaus and Bradley, 1958) have been constructed, but these are based upon indirect measurements of CO$_2$ via changes in pH using a pH-sensitive transducer embedded in a small reservoir with bicarbonate and carbonic anhydrase added to speed up hydration of CO$_2$ (De Beer *et al.*, 1997). These sensors are, however, sluggish at low concentrations and respond to external CO$_2$ in a logarithmic fashion with a poor resolution at high CO$_2$ concentrations; all these factors severely limited application of such sensors. The breakthrough in the field was recently achieved by producing a novel amperometric CO$_2$ microsensor with a linear response to external CO$_2$. This sensor has a typical tip size of 30 μm and responds linearly from the detection limit of 0.0005 kPa and up to 5 kPa pCO$_2$ (Revsbech *et al.*, 2019).

Recent applications of CO$_2$ microsensors in plant biology

CO$_2$ exchange of plant tissues with the environment is routinely measured using infrared gas analysers (IRGAs), and the intercellular CO$_2$ concentration can be inferred based on stomatal conductance (Long and Bernacchi, 2003). In stark contrast, the tissue concentration can be directly measured with the CO$_2$ microsensor.

Box 2. A minute hypoxic niche of stem cells revealed with a 3 µm O_2 microsensor

In the study by Weits *et al.* (2019), a customized O_2 microsensor was used to demonstrate the presence of a hypoxic niche in the shoot apical meristem of Arabidopsis. The presence of a hypoxic tissue was inferred early on by hypoxic reporters, namely a group of genes and their associated transcription factors that normally are only expressed during hypoxic conditions in the tissues (Licausi *et al.*, 2011).

However, actual tissue measurements of molecular O_2 were lacking, and custom-built microsensors with a tip diameter of only 3 µm were constructed to obtain convincing O_2 measurements in intact tissues. These measurements revealed the existence of a hypoxic group of ~30 cells within the shoot apical meristem of 4-day-old Arabidopsis. Oxygen partial pressure (pO_2) declined steeply from levels around air equilibrium to 5–7 kPa within a distance of only 10–20 µm. In the hypoxic niche, low oxygen levels control the rate at which new leaves are produced by promoting the stability of a protein, named ZPR2, responsible for cell proliferation and differentiation. Hypoxia within the group of stem cells is required to keep the meristem in a functional state; hyperoxia resulted in cessation of leaf production from the shoot apical meristem.
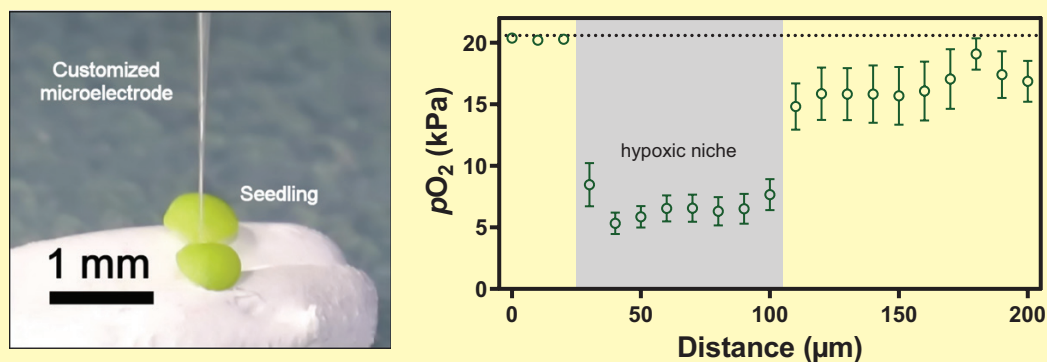
The world's smallest Clark-type O_2 microsensor inserted into the shoot apical meristems of a 4-day-old Arabidopsis seedling (left) and the resulting tissue O_2 profile (right) revealing a hypoxic niche enveloping the stem cells of the meristem. Data are means ±SE, *n*=5; modified from Weits *et al.*, (2019).

The novel CO_2 microsensor was used in a combination with a conventional O_2 microsensor to elucidate leaf tissue CO_2 and O_2 dynamics of a C_3 and a CAM (crassulacean acid metabolism) plant with high temporal resolution (Pedersen *et al.*, 2018). The study showed that during the night, pCO_2 accumulated inside the leaves of the C_3 plant and reached 3.5 kPa. In the CAM plant, fixation into malate kept CO_2 near the detection limit of the sensor during most of the dark period until the carboxylation capacity was reached, whereafter CO_2 also increased in the CAM plant. Night-time leaf pO_2 was below air equilibrium in both the C_3 and the CAM plant, with pO_2 approaching anoxia in the C_3 plant. During the day, CO_2 was rapidly depleted in the C_3 plant but was high in the CAM plant as a result of decarboxylation of malate. Interestingly, leaf pO_2 of the C_3 plant peaked in the presence of the accumulated respiratory CO_2 but declined rapidly as this source of CO_2 was again depleted. The temporal resolution obtained in the study was unparalleled and revealed new insight into the exciting contrast between C_3 and CAM photosynthesis as related to tissue CO_2 and O_2 dynamics.

In addition to providing the first radial concentration profiles of CO_2 in roots (Box 3), the CO_2 sensor was also recently used to establish fluxes of respiratory CO_2 between the roots and the surrounding medium (Colmer *et al.*, 2020). Based on simultaneous measurements of CO_2 and O_2 in the diffusive boundary layer enveloping the root (figure in Box 1), the CO_2 efflux can be calculated using a modified version of Fick's First Law (Henriksen *et al.*, 1992). The study showed that the respiratory quotient of the roots increased from slightly above 1 with external O_2 in the liquid medium at air equilibrium, to ~5 when the external O_2 supply was lowered to 3.7 kPa.

Finally, the use of the novel CO_2 microsensor has revealed that a dense layer of epiphytes on leaves of seagrasses greatly depletes CO_2 as the leaf and the microalgae compete for CO_2 during the light (Brodersen *et al.*, 2020). It was also shown that CO_2 accumulated near the leaf surface during darkness since the epiphytic microalgae extend the diffusive boundary layer and thereby increase the diffusive resistance to CO_2 exchange with the surrounding seawater.

Sulfide (H_2S)

The chemical equilibrium of sulfides is mainly controlled by pH so that gaseous H_2S dominates at low pH, with the ionic forms (HS^- and S^{2-}) dominating at neutral and high pH.

Box 3. Radial O_2 and CO_2 concentration profiles in roots of chickpea

The construction of a novel CO_2 microsensor has enabled measurements of tissue-specific concentrations of CO_2 in plant tissues (Pedersen *et al.*, 2018; Colmer *et al.*, 2020). Radial O_2 profiles have been taken from roots of monocots or dicots for a number of years, but the associated CO_2 concentration profiles were not known.

Using roots of 7-day-old chickpea seedlings, measurements of CO_2 and O_2 revealed very contrasting radial concentration profiles. For CO_2, the concentration increased towards the root surface since CO_2 was being produced in respiration and/or fermentation. Inside the cortex, the concentration profile was relatively flat due to the high diffusivity in the porous tissues and the concentration again rose inside the stele where porosity was low and where the produced CO_2 then had a tendency to accumulate. For O_2, the situation was the opposite, with high external O_2 concentrations that declined toward the root surface but again showing a flat radial concentration profile in the porous cortex; the stele was severely hypoxic/anoxic due to low diffusivity and high consumption of O_2.

Moreover based on concentration gradients in the diffusive boundary layer, the application of the CO_2 sensor also enabled measurements of fluxes as CO_2 diffused from the root tissues to the surrounding medium. These measurements revealed interesting patterns in the respiratory quotient when the external O_2 supply became rate limiting for oxic respiration (see text).
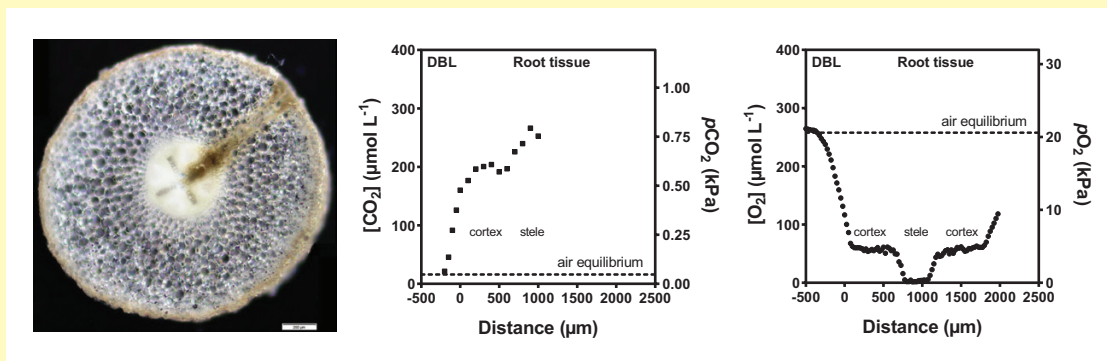
Cross-section of a chickpea root showing the scar left by the CO_2 microsensor (left). The sensor penetrated the root surface and stopped in the centre of the stele. Radial tissue CO_2 and O_2 profiles also from a chickpea root measured in experimental condition mimicking waterlogging (right); modified from Colmer *et al.* (2020).

Microsensors are available for H_2S as well as for S^{2-} (Kühl and Steuckart, 2000) but, in plant biology, emphasis has been on H_2S since the gas can diffuse and spread quickly in porous tissues and aerenchyma the same way as O_2 and CO_2 (Pedersen *et al.*, 2004).

The study of H_2S intrusion into roots of seagrasses has long had high priority in seagrass research since H_2S poisoning is suspected to play a key role in die-back events observed globally (Koch *et al.*, 2007). In the sea bottom, sulfides are produced by sulfate-reducing bacteria, but a microshield of O_2 resulting from the radial O_2 loss (ROL) from the roots can oxidize sulfides before these enter the belowground tissues (Brodersen *et al.*, 2015, 2018); see Fig. 1 for an example of microsensors in action inside a stand of seagrasses. However, poor O_2 status of the roots can result in H_2S intrusion that spreads to tissues that are sensitive to H_2S poisoning (Johnson *et al.*, 2018). Recent field studies revealed that deposition of fine clay particles, resulting in decreased photosynthesis during the day (due to shading) and high resistance to O_2 uptake

during the night (due to thicker diffusive boundary layers), can lead to a critically low O_2 status of the roots followed by H_2S intrusion that subsequently spreads to the sensitive shoot meristem (Brodersen *et al.*, 2017). Moreover, H_2S can also play a role in breaking seed dormancy (Corpas *et al.*, 2019) but, to our knowledge, measurements of internal concentrations of H_2S in seeds are still lacking.

Ionic analytes

Monitoring changes in intracellular ion concentrations is essential not only for diagnostics of plant nutritional status but also for understanding mechanisms of plant responses to adverse environmental conditions. Traditionally, cytosolic free Ca^{2+} has been considered as an important 'second messenger' mediating a broad range of adaptive and developmental responses in plants (Konrad *et al.*, 2018). Recently, changes in cellular K^+ (Rubio *et al.*, 2020; Shabala, 2017), nitrate (Vega

Box 4. The MIFE technique for non-invasive ion flux measurements
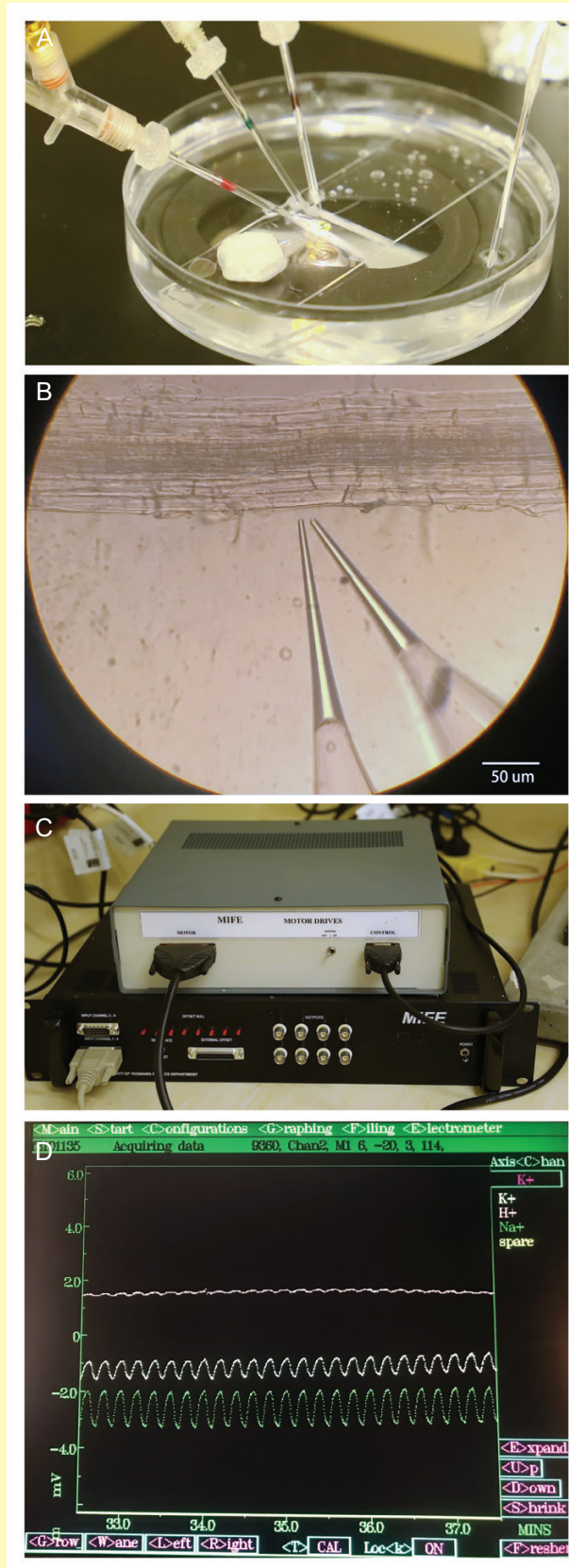

The MIFE technique enables measuring kinetics of net ion fluxes across cellular membranes with high temporal (5 s) and spatial (several micrometres) resolution. Microelectrodes are pulled

from borosilicate glass capillaries to have a tip diameter of ~2 μm. Electrodes are back-filled with an appropriate solution and then front-filled with commercially available cocktails. Electrodes are then mounted on a multi-manipulator providing 3-dimensional positioning and calibrated in the set of standards, specific for each ion. The plant specimen is immobilized in the measuring chamber (e.g. Petri dish; panel A), and electrodes are positioned next to the specimen (e.g. mature epidermis of Arabidopsis root; panel B) at a small distance (typically ranging between 10 μm and 50 μm, depending on the heterogeneity of the tissue). This distance is small for the single-cell measurements (e.g. isolated protoplast or vacuole, root hair, guard cell, or pollen tube) and larger for more homogenous multicellular tissues such as root epidermis or leaf mesophyll. During measurement, electrodes are moved in a square-wave manner (default setting 5 s/5 s cycle) by a computer-driven stepper motor using a hydraulic manipulator, between the initial position and another one, 20–50 μm further away. Signals from each electrode are amplified and digitized by MIFE electronics (panel C). The data acquisition is done by the CHART software, and the process is visualized on the screen (panel D). The difference in electrode recordings between two positions (measured in milli Volts) is a proxy for a concentration gradient and proportional to the magnitude of the flux. If an ion is taken up by a plant cell, then the concentration at position 1 (closer to specimen) will be lower than that at position 2 (further away). Vice versa, if an ion is expelled then its concentration in the proximity of the cell will be higher. After the conclusion of the experiment, the values of net fluxes across the tissue boundary (expressed in nmol m^{-2} s^{-1}) are calculated from the recorded data using appropriate diffusion geometry profiles (e.g. cylindrical for the root, planar for the leaf mesophyll, or spherical for the protoplast). The first 1–2 s after the movement began were ignored to allow for both the movement (0.3 s) and the electrochemical settling of the electrodes (Shabala *et al.*, 1997).


Box 5. Combining microelectrode ion flux measurements with other electrophysiological and imaging techniques

The power of the microelectrode ion-measuring technique is increased dramatically when combined with other electrophysiological or imaging methods. This is illustrated by several examples below. The first combination of the MIFE and patch–clamp method was published ~20 years ago (Tyerman *et al.*, 2001). Being applied to protoplasts isolated from wheat root cortex, and combining MIFE H^{+} flux measurements with records of the reversal potential difference (measured in the current clamp mode in the whole-cell patch configuration), this work has revealed the critical role of the H^{+}-ATPase pump in generating sustained 40–60 min period oscillations in root cells (panel A).
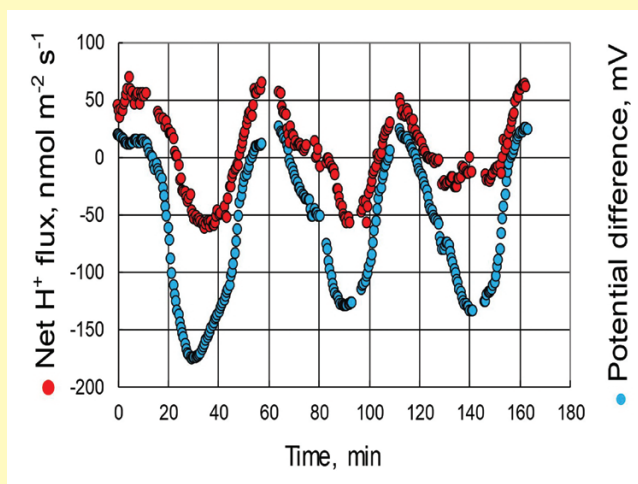

(A) Oscillations in net H^{+} fluxes (red) and resting potential difference (blue) recorded in the current clamp mode from wheat cortical root protoplasts. The resting potential difference oscillated in phase with the oscillations in net H^{+} flux and was fully suppressed by vanadate (a known H^{+}-ATPase inhibitor). Based on Tyerman *et al.*, (2001).

At about the same time, the MIFE technique was combined, for the first time, with the voltage–clamp method, to understand the role of voltage-gated K$^+$ channels in Arabidopsis root responses to low pH stress (Babourina *et al.*, 2001).
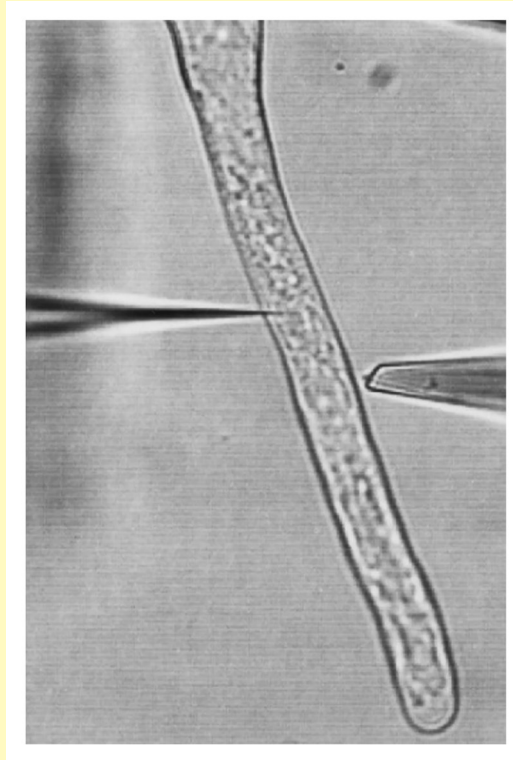
(B) An Arabidopsis root hair with an impaled double-barrelled microelectrode (left) for voltage—clamp and current measurements and a MIFE ion-selective K$^+$ electrode located several micrometres from the root hair surface (right). From Babourina *et al*. (2001).

More recently, combination of MIFE and fluorescence dye confocal imaging was used to reveal the role of the meristem as a potential salt sensor in plant roots (Wu *et al.*, 2018). While SOS1-mediated net Na$^+$ efflux from the elongation zone showed strong correlation with genotypic and interspecific difference in salt tolerance, tolerant genotypes and species have accumulated much more Na in the root meristem (panel C).
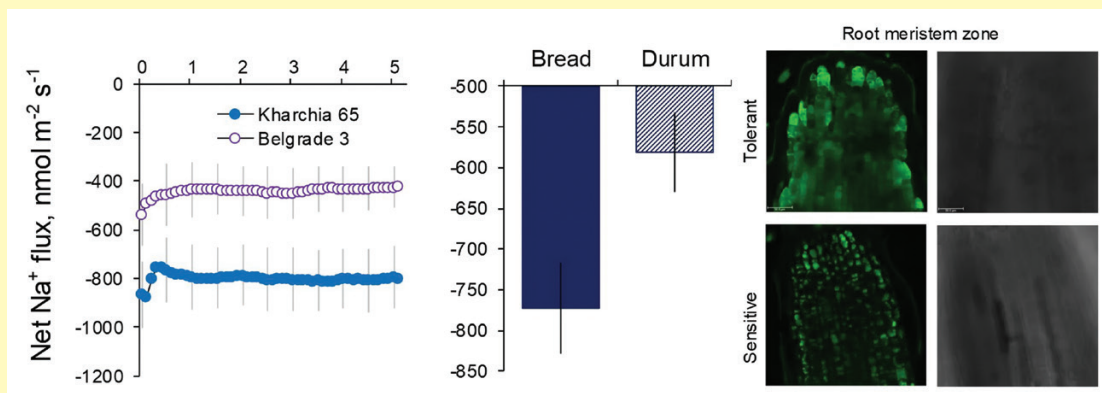
(C) Net Na$^+$ fluxes measured from the elongation root zone of two bread wheat genotypes contrasting in salinity stress tolerance (Kharchia 65, tolerant; Belgrade 3 sensitive; left panel). This efflux is mediated by the SOS1 Na$^+$/H$^+$ exchanger and explains the genotypic difference in salt tolerance between bread and durum wheat (central panel). However, the intensity of CoroNa Green fluorescence dye was much stronger in the meristematic cells in tolerant genotypes (right panel), indicating high specificity of cellular responses to salinity. From Wu *et al*. (2018).
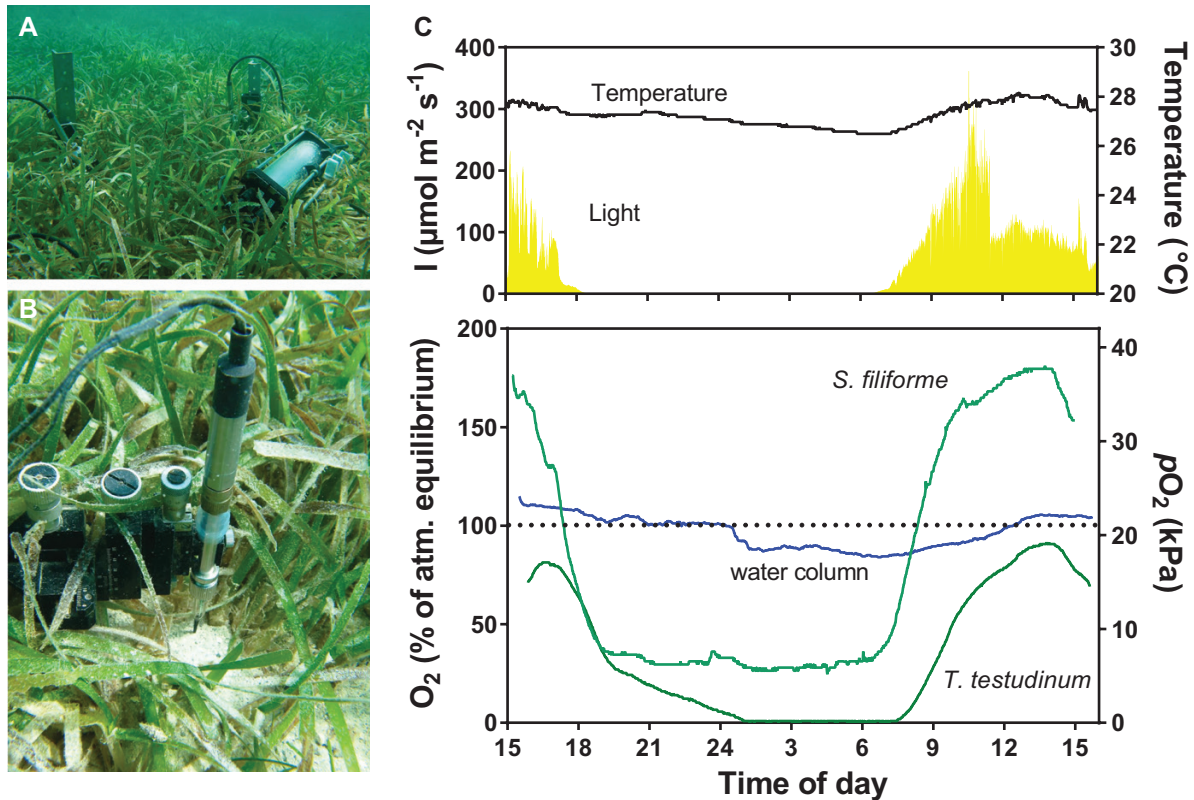
Fig. 1. Microsensors enable *in situ* tissue measurements of, for example, tissue O_2 and H_2S dynamics under field conditions. The photos show oxygen and sulfide microsensors inserted into the rhizome of the seagrass, *Thalassia testudinum*, at 6 m depth in the Caribbean. (A) The electronic amplifier and two replicate set-ups and (B) details of one set-up with a micromanipulator and microsensor. (C) The type of data that can be obtained from *in situ* deployments of microsensors where light and temperature fluctuate over a diel cycle (C, upper panel) and the resulting internal O_2 dynamics in the belowground rhizomes of the seagrasses, *T. testudinum* and *Syringodium filiforme* (C, lower panel). (C) is reprinted from Holmer *et al.* (2009), Sulfide intrusion in the tropical seagrasses *Thalassia testudinum* and *Syringodium filiforme*. Estuarine Coastal and Shelf Science 85: 319–326, Copyright (2009), with permission from Elsevier.

et al., 2019), and ammonium (Liu and von Wirén, 2017) have been added to the list of known 'second messengers'. These signalling molecules then direct changes in gene expression affecting plant metabolism, growth, and development. Importantly, such signalling (and consequent transcriptional and physiological changes) operates in a strict tissue- and cell-specific manner, prompting the need to monitor changes in cellular ion concentrations or fluxes with a high spatial resolution. Ion-selective microsensors fully satisfy this requirement.

The most popular type of ion-selective microsensors are potentiometric electrodes that use LIXs. Such a LIX (also known as an ionophore) is a neutral macrocyclic ion carrier that is dissolved in a viscous organic liquid membrane. When the LIX 'traps' the analyte at the interface between the solution and membrane, the charge separation occurs, leading to changes in a phase boundary potential that is recorded and then converted into ion concentration. For intracellular ion measurement, the appropriate LIX must be imbedded into a membrane matrix, because cell turgor will displace a liquid membrane from the electrode tip, thereby changing or eliminating the sensitivity to the measuring ion. The matrix used is usually a high molecular weight poly(vinyl chloride), but can include other polymers, such as nitrocellulose for additional strength (Miller and Smith, 2012). Also, a simultaneous recording of membrane potential is required

for quantification of the concentration of the ion in question. Thus, such intracellular ion concentration measurements are conducted by the double-barrelled microelectrodes, with one barrel containing a specific ion-selective LIX, and another one used for voltage recording. Fabrication of such double-barrelled microelectrodes is not a trivial task; this explains the relatively small number of studies using this technique. Another confounding factor is a difficulty with impalement, with the electrode tip often being blocked by the dense cytosol, or the impalement being rapidly lost (in fast-growing tissues such as root or shoot apical parts).

A very effective way to overcome the above limitations of the impaled method is to use non-invasive ion-selective microelectrodes to measure net fluxes of ions across the cellular membranes. Three concurrent systems have been developed and became commercially available for users: (i) the MIFE system designed and manufactured by the University of Tasmania (Shabala *et al.*, 1997; Shabala *et al.*, 2006); (ii) the SIET (Scanning Ion-Electrode Technique) system; and (iii) the NMT (Nutrient Micro-Test) system (a commercial service provided by Xuyue BioFunction Institute in Beijing). While each of these systems uses different hardware and software (see Newman *et al.*, 2012 for comparative analysis), the major principle is the same. Each method uses ion-selective microelectrodes that are moved between two positions: close

to, and further from, the cellular membrane (Box 4). The system then records the voltage gradient between two positions and converts it into concentration parameters using the calibrated Nernst slopes of the electrodes. Net fluxes of specific ions are then calculated based on specific diffusion profiles that reflect the specimen geometry (e.g. cylindrical for a root or pollen tube, or spherical for an isolated protoplast or vacuole). The travel range is set by the user and is typically in a range of 10–50 μm depending on the specimen. The time required for the electrode to move from one position to another and reach steady readings is typically ~1.5–2 s (Shabala *et al.*, 1997); this sets up the practical limit on the time resolution of this method.

The current Sigma–Aldrich catalogue has >100 entries for LIXs (ionophores); this includes most of the essential macro- (K, Ca, Mg, NH_4, NO_3, and SO_4) and micro- (Cu, Zn, Cl, and Ni) analytes. Toxic elements such as Na^+ (causing salinity stress) and heavy metals (Cd, Hg, and Pb) can also be measured. As a result, the non-invasive ion flux measuring technology is now accepted as a standard tool for *in situ* studies of membrane transport processes in living organisms that has resulted in >1000 publications. The power of this method is increased dramatically when combined with other powerful biophysical methods (Box 5). For example, its combination with the patch–clamp method enabled understanding of the role of specific transport proteins in plant responses to salinity (Shabala *et al.*, 2016; Zeng *et al.*, 2018) and oxidative stress (Demidchik *et al.*, 2010; Pottosin *et al.*, 2018). Similarly, combination of the MIFE method with TEVC (two-electrode voltage clamping) has been shown to be a powerful tool to understand the role of γ-aminobutyric acid (GABA) as an important signalling molecule that negatively regulates aluminium-activated malate transporter (ALMT) proteins (Ramesh *et al.*, 2015). A further application of the MIFE technique to a range of Arabidopsis transport mutants has moreover revealed that GABA also operates upstream of H^+-ATPase and controls cytosolic K^+ homeostasis in plant cells (Su *et al.*, 2019). Combination of non-invasive ion flux measurements with the single-cell pressure probe has provided direct evidence for the role of inorganic ion uptake in plant osmotic adjustment (Shabala and Lew, 2002). Moreover, the combination of the MIFE, carbon fibre amperometry, and MRI led to understanding of regulation of endocytosis in the Venus flytrap (*Dionaea muscipula*) secretory glands (Scherzer *et al.*, 2017). By the concurrent use of the MIFE and fluorescent dye imaging techniques, the mechanistic basis of cell-specific signalling and adaptive responses to salinity (Wu *et al.*, 2018; Wu *et al.*, 2019) and hypoxia (Wang *et al.*, 2017, 2019) and a new technology platform for cell-based plant phenotyping has been developed and demonstrated (Gill *et al.*, 2018; Wang *et al.*, 2019).

Conclusions and outlook

Commercially available NO or H_2O_2 microsensors have not yet been applied in plant biology even though these two analytes play crucial roles as regulatory or signalling molecules (Slesak *et al.*,

2007; Wany *et al.*, 2017). Consequently, we foresee future studies where indirect discrete measurements of, for example, NO using fluorescent probes (Hartman *et al.*, 2019) are supplemented with direct concentration measurements of the target analyte.

We predict that the novel CO_2 microsensor holds a great potential to further advance our understanding of plant tissue CO_2 dynamics when it eventually becomes commercially available. CO_2 exchange of leaves with the environment is currently measured using an IRGA and, based on stomatal conductance, the tissue CO_2 concentration can be estimated. The inferred tissue pCO_2 is sometimes checked by means of discrete sampling of tissue gases and subsequent analysis. However, the sampling is destructive, remains discrete, and has poor spatial resolution. Furthermore, the CO_2 microsensor holds the potential to establish tissue-specific resistances to CO_2 diffusion.

The two major hurdles limiting application of ion-selective microsensors in plant biology research is a need for a custom-made manufacturing of microelectrode probes on a daily basis, but also the poor selectivity of some of the commercial LIXs. The latter is especially crucial for salinity research studies, as all commercially available Na^+ ionophores are also highly sensitive to K^+ and Ca^{2+} (Chen *et al.*, 2005). This problem can, however, be overcome by using custom-made calixarene-based microelectrodes with improved Na^+ selectivity (Jayakannan *et al.*, 2011). The selectivity of all Mg and Zn ionophores is also poor and interferes with other divalent cations present in solution. Currently, the issue is dealt with by calibrating the electrodes in two sets of calibration solutions—one for the analyte in question, another one for the interfering ion—followed by complex computational procedures accounting for non-ideal selectivity (Knowles and Shabala, 2004). A possible way forward is to design optical microsensors based on fluorescence that have much better selectivity as illustrated for Zn (e.g. by Kumar *et al.* 2018). Finally, an obvious ommision from the list of commercially available LIXs is a phosphate ionophore. Modern agriculture relies heavily on the use of a rock phosphate, whose consumption has increased 4-fold since the beginning of a Green Revolution (Childers *et al.*, 2011). However, rock phosphate is a non-renewable resource and may be completely exhausted in 50–200 years (Baker *et al.*, 2015). Designing a highly selective phosphate microsensor may be essential in assisting plant breeders in creating varieties with high P use efficiency, thus minimizing demands for this nutrient and reducing the environmental footprint of P fertilization on natural ecosystems.

Acknowledgements

References

Alova A, Erofeev A, Gorelkin P, Bibikova T, Korchev Y, Majouga A, Bulychev A. 2020. Prolonged oxygen depletion in microwounded cells

of *Chara corallina* detected with novel oxygen nanosensors. Journal of Experimental Botany **71**, 386–398.

Andersen K, Kjær T, Revsbech NP. 2001. An oxygen insensitive microsensor for nitrous oxide. Sensors and Actuators B: Chemical **81**, 42–48.

Anwar A, Li Y, He C, Yu X. 2019. 24-Epibrassinolide promotes NO_3^- and NH_4^+ ion flux rate and NRT1 gene expression in cucumber under sub-optimal root zone temperature. BMC Plant Biology **19**, 225.

Armstrong W, Beckett PM, Colmer TD, Setter TL, Greenway H. 2019. Tolerance of roots to low oxygen: 'anoxic' cores, the phytoglobin–nitric oxide cycle, and energy or oxygen sensing. Journal of Plant Physiology **239**, 92–108.

Babourina O, Hawkins B, Lew RR, Newman I, Shabala S. 2001. K^+ transport by Arabidopsis root hairs at low pH. Australian Journal of Plant Physiology **28**, 637–643.

Baker A, Ceasar SA, Palmer AJ, Paterson JB, Qi W, Muench SP, Baldwin SA. 2015. Replace, reuse, recycle: improving the sustainable use of phosphorus by plants. Journal of Experimental Botany **66**, 3523–3540.

Brodersen KE, Hammer KJ, Schrameyer V, Floytrup A, Rasheed MA, Ralph PJ, Kühl M, Pedersen O. 2017. Sediment resuspension and deposition on seagrass leaves impedes internal plant aeration and promotes phytotoxic H_2S intrusion. Frontiers in Plant Science **8**, 657.

Brodersen KE, Koren K, Revsbech NP, Kühl M. 2020. Strong leaf surface basification and CO_2 limitation of seagrass induced by epiphytic biofilm microenvironments. Plant, Cell & Environment **43**, 174–187.

Brodersen KE, Nielsen DA, Ralph PJ, Kühl M. 2015. Oxic microshield and local pH enhancement protects *Zostera muelleri* from sediment derived hydrogen sulphide. New Phytologist **205**, 1264–1276.

Brodersen KE, Siboni N, Nielsen DA, Pernice M, Ralph PJ, Seymour J, Kühl M. 2018. Seagrass rhizosphere microenvironment alters plant-associated microbial community composition. Environmental Microbiology **20**, 2854–2864.

Chen Z, Newman I, Zhou M, Mendham N, Zhang G, Shabala S. 2005. Screening plants for salt tolerance by measuring K^+ flux: a case study for barley. Plant, Cell & Environment **28**, 1230–1246.

Childers DL, Corman J, Edwards M, Elser JJ. 2011. Sustainability challenges of phosphorus and food: solutions from closing the human phosphorus cycle. BioScience **61**, 117–124.

Clark LC Jr. 1956. Monitor and control of blood and tissue oxygen tensions. Transactions of the American Society of Artificial Internal Organs **2**, 41–48.

Colmer TD, Winkel A, Kotula L, Armstrong W, Revsbech NP, Pedersen O. 2020. Root O_2 consumption, CO_2 production and tissue concentration profiles in chickpea, as influenced by environmental hypoxia. New Phytologist **226**, 373–384.

Corpas FJ, González-Gordo S, Cañas A, Palma JM. 2019. Nitric oxide and hydrogen sulfide in plants: which comes first? Journal of Experimental Botany **70**, 4391–4404.

Damgaard LR, Revsbech NP. 1997. A microscale biosensor for methane containing methanotrophic bacteria and an internal oxygen reservoir. Analytical Chemistry **69**, 2262–2267.

De Beer D, Glud A, Epping E, Kuhl M. 1997. A fast-responding CO_2 microelectrode for profiling sediments, microbial mats, and biofilms. Limnology and Oceanography **42**, 1590–1600.

Demidchik V, Cuin TA, Svistunenko D, Smith SJ, Miller AJ, Shabala S, Sokolik A, Yurin V. 2010. Arabidopsis root K^+-efflux conductance activated by hydroxyl radicals: single-channel properties, genetic basis and involvement in stress-induced cell death. Journal of Cell Science **123**, 1468–1479.

Gill MB, Zeng F, Shabala L, Böhm J, Zhang G, Zhou M, Shabala S. 2018. The ability to regulate voltage-gated K^+-permeable channels in the mature root epidermis is essential for waterlogging tolerance in barley. Journal of Experimental Botany **69**, 667–680.

Gundersen JK, Ramsing NB, Glud RN. 1998. Predicting the signal of O_2 microsensors from physical dimensions, temperature, salinity, and O_2 concentration. Limnology and Oceanography **43**, 1932–1937.

Hartman S, Liu Z, van Veen H, et al. 2019. Ethylene-mediated nitric oxide depletion pre-adapts plants to hypoxia stress. Nature Communications **10**, 4020.

Henriksen GH, Raman DR, Walker LP, Spanswick RM. 1992. Measurement of net fluxes of ammonium and nitrate at the surface of barley roots using ion-selective microelectrodes: II. Patterns of uptake along the root axis and evaluation of the microelectrode flux estimation technique. Plant Physiology **99**, 734–747.

Holmer M, Pedersen O, Krause-Jensen D, Olesen B, Petersen MH, Schopmeyer S, Koch M, Lomstein BA, Jensen HS. 2009. Sulfide intrusion in the tropical seagrasses *Thalassia testudinum* and *Syringodium filiforme*. Estuarine Coastal and Shelf Science **85**, 319–326.

Huang Y, Cao H, Yang L, et al. 2019. Tissue-specific respiratory burst oxidase homolog-dependent H_2O_2 signaling to the plasma membrane H^+-ATPase confers potassium uptake and salinity tolerance in Cucurbitaceae. Journal of Experimental Botany **70**, 5879–5893.

Jayakannan M, Babourina O, Rengel Z. 2011. Improved measurements of Na^+ fluxes in plants using calixarene-based microelectrodes. Journal of Plant Physiology **168**, 1045–1051.

Johnson CR, Koch MS, Pedersen O, Madden CJ. 2018. Hypersalinity as a trigger of seagrass die off events in Florida Bay: evidence based on meristem O_2 and H_2S dynamics. Journal of Experimental Marine Biology and Ecology **504**, 47–52.

Klimant I, Kühl M, Glud RN, Holst G. 1997. Optical measurement of oxygen and temperature in microscale: strategies and biological applications. Sensors and Actuators B: Chemical **38**, 29–37.

Knowles A, Shabala S. 2004. Overcoming the problem of non-ideal liquid ion exchanger selectivity in microelectrode ion flux measurements. Journal of Membrane Biology **202**, 51–59.

Koch MS, Schopmeyer SA, Nielsen OI, Kyhn-Hansen C, Madden CJ. 2007. Conceptual model of seagrass die-off in Florida Bay: links to biogeochemical processes. Journal of Experimental Marine Biology and Ecology **350**, 73–88.

Konrad KR, Maierhofer T, Hedrich R. 2018. Spatio-temporal aspects of Ca^{2+} signalling: lessons from guard cells and pollen tubes. Journal of Experimental Botany **69**, 4195–4214.

Koren K, Jensen PØ, Kühl M. 2016. Development of a rechargeable optical hydrogen peroxide sensor—sensor design and biological application. The Analyst **141**, 4332–4339.

Kühl M, Steuckart C. 2000. Sensors for in situ analysis of sulfide in aquatic systems. In: Buffle J, Horvai G, eds. In situ monitoring of aquatic systems: chemical analysis and speciation. New York: Wiley, 121–159.

Kulagina NV, Michael AC. 2003. Monitoring hydrogen peroxide in the extracellular space of the brain with amperometric microsensors. Analytical Chemistry **75**, 4875–4881.

Kumar RS, Kumar SKA, Vijayakrishna K, Sivaramakrishna A, Paira P, Rao CVSB, Sivaraman N, Sahoo SK. 2018. Bipyridine bisphosphonate-based fluorescent optical sensor and optode for selective detection of Zn^{2+} ions and its applications. New Journal of Chemistry **42**, 8494–8502.

Lassen C, Glud RN, Ramsing NB, Revsbech NP. 1998. A method to improve the spatial resolution of photosynthetic rates obtained by oxygen microsensors. Journal of Phycology **34**, 89–93.

Lassen C, Ploug H, Jørgensen BB. 1992. A fibre-optic scalar irradiance microsensor: application for spectral light measurements in sediments. FEMS Microbiology Letters **86**, 247–254.

Lassen C, Revsbech NP, Pedersen O. 1997. Macrophyte development and resuspension regulate the photosynthesis and production of benthic microalgae. Hydrobiologia **350**, 1–11.

Lehner P, Larndorfer C, Garcia-Robledo E, Larsen M, Borisov SM, Revsbech NP, Glud RN, Canfield DE, Klimant I. 2015. LUMOS—a sensitive and reliable optode system for measuring dissolved oxygen in the nanomolar range. PLoS One **10**, e0128125.

Li X, Li Y, Mai J, et al. 2018. Boron alleviates aluminum toxicity by promoting root alkalization in transition zone via polar auxin transport. Plant Physiology **177**, 1254–1266.

Licausi F, Weits DA, Pant BD, Scheible WR, Geigenberger P, van Dongen JT. 2011. Hypoxia responsive gene expression is mediated by various subsets of transcription factors and miRNAs that are determined by the actual oxygen availability. New Phytologist **190**, 442–456.

Liu J, Shabala S, Shabala L, Zhou M, Meinke H, Venkataraman G, Chen Z, Zeng F, Zhao Q. 2019. Tissue-specific regulation of Na^+ and K^+ transporters explains genotypic differences in salinity stress tolerance in rice. Frontiers in Plant Science **10**, 1361.

Liu Y, von Wirén N. 2017. Ammonium as a signal for physiological and morphological responses in plants. Journal of Experimental Botany **68**, 2581–2592.

Long SP, Bernacchi CJ. 2003. Gas exchange measurements, what can they tell us about the underlying limitations to photosynthesis? Procedures and sources of error. Journal of Experimental Botany **54**, 2393–2401.

Meng XM, Huang X, Lu HL, Zhang CM, Kim YC, Chen J, Xu WX. 2017. H_2S-induced gastric fundus smooth muscle tension potentiation is mediated by the phosphoinositide 3-kinase/Akt/endothelial nitric oxide synthase pathway. Experimental Physiology **102**, 779–790.

Miller AJ, Smith S. 2012. Measuring intracellular ion concentrations with multi-barrelled microelectrodes. Methods in Molecular Biology **913**, 67–77.

Mori Y, Kurokawa Y, Koike M, Malik AI, Colmer TD, Ashikari M, Pedersen O, Nagai K. 2019. Diel O_2 dynamics in partially and completely submerged deepwater rice: leaf gas films enhance internodal O_2 status, influence gene expression, and accelerate stem elongation for 'snorkelling' during submergence. Plant & Cell Physiology **65**, 973–985.

Newman I, Chen SL, Porterfield DM, Sun J. 2012. Non-invasive flux measurements using microsensors: theory, limitations, and systems. Methods in Molecular Biology **913**, 101–117.

Pedersen O, Binzer T, Borum J. 2004. Sulphide intrusion in eelgrass (*Zostera marina* L.). Plant, Cell & Environment **27**, 595–602.

Pedersen O, Colmer TD, Borum J, Zavala-Perez A, Kendrick GA. 2016. Heat stress of two tropical seagrass species during low tides—impact on underwater net photosynthesis, dark respiration and diel *in situ* internal aeration. New Phytologist **210**, 1207–1218.

Pedersen O, Colmer TD, Garcia-Robledo E, Revsbech NP. 2018. CO_2 and O_2 dynamics in leaves of aquatic plants with C_3 or CAM photosynthesis—application of a novel CO_2 microsensor. Annals of Botany **122**, 605–615.

Pedersen O, Nakayama Y, Yasue H, Kurokawa Y, Takahashi H, Floytrup AH, Omori F, Mano Y, Colmer TD, Nakazono M. 2020. Lateral roots, in addition to the adventitious roots, form a barrier to radial oxygen loss in *Zea nicaraguensis* and a chromosome segment introgression line in maize. New Phytologist doi: 10.1111/nph.16452.

Pottosin I, Wherrett T, Shabala S. 2009. SV channels dominate the vacuolar Ca^{2+} release during intracellular signaling. FEBS Letters **583**, 921–926.

Pottosin I, Zepeda-Jazo I, Bose J, Shabala S. 2018. An anion conductance, the essential component of the hydroxyl-radical-induced ion current in plant roots. International Journal of Molecular Sciences **19**, 897.

Ramesh SA, Tyerman SD, Xu B, et al. 2015. GABA signalling modulates plant growth by directly regulating the activity of plant-specific anion transporters. Nature Communications **6**, 7879.

Revsbech NP. 1989. An oxygen microelectrode with a guard cathode. Limnology and Oceanography **34**, 474–478.

Revsbech NP, Garcia-Robledo E, Sveegaard S, Andersen MH, Gothelf KV, Larsen LH. 2019. Amperometic microsensor for measurement of gaseous and dissolved CO_2. Sensors and Actuators B: Chemical **283**, 349–354.

Rubio F, Nieves-Cordones M, Horie T, Shabala S. 2020. Doing 'business as usual' comes with a cost: evaluating energy cost of maintaining plant intracellular K^+ homeostasis under saline conditions. New Phytologist **225**, 1097–1104.

Sa G, Yao J, Deng C, et al. 2019. Amelioration of nitrate uptake under salt stress by ectomycorrhiza with and without a Hartig net. New Phytologist **222**, 1951–1964.

Sadanandom A, Napier RM. 2010. Biosensors in plants. Current Opinion in Plant Biology **13**, 736–743.

Scherzer S, Shabala L, Hedrich B, et al. 2017. Insect haptoelectrical stimulation of Venus flytrap triggers exocytosis in gland cells. Proceedings of the National Academy of Sciences, USA **114**, 4822–4827.

Severinghaus JW, Bradley AF. 1958. Electrodes for blood pO_2 and pCO_2 determination. Journal of Applied Physiology **13**, 515–520.

Shabala L, Ross T, McMeekin T, Shabala S. 2006. Non-invasive microelectrode ion flux measurements to study adaptive responses of microorganisms to the environment. FEMS Microbiology Reviews **30**, 472–486.

Shabala L, Zhang J, Pottosin I, et al. 2016. Cell-type-specific H^+-ATPase activity in root tissues enables K^+ retention and mediates acclimation of barley (*Hordeum vulgare*) to salinity stress. Plant Physiology **172**, 2445–2458.

Shabala S. 2017. Signalling by potassium: another second messenger to add to the list? Journal of Experimental Botany **68**, 4003–4007.

Shabala SN, Lew RR. 2002. Turgor regulation in osmotically stressed *Arabidopsis* epidermal root cells. Direct support for the role of inorganic ion uptake as revealed by concurrent flux and cell turgor measurements. Plant Physiology **129**, 290–299.

Shabala SN, Newman IA, Morris J. 1997. Oscillations in H^+ and Ca^{2+} ion fluxes around the elongation region of corn roots and effects of external pH. Plant Physiology **113**, 111–118.

Sheng H, Ma J, Pu J, Wang L. 2018. Cell wall-bound silicon optimizes ammonium uptake and metabolism in rice cells. Annals of Botany **122**, 303–313.

Slesak I, Libik M, Karpinska B, Karpinski S, Miszalski Z. 2007. The role of hydrogen peroxide in regulation of plant metabolism and cellular signalling in response to environmental stresses. Acta Biochimica Polonica **54**, 39–50.

Su N, Wu Q, Chen J, Shabala L, Mithöfer A, Wang H, Qu M, Yu M, Cui J, Shabala S. 2019. GABA operates upstream of H^+-ATPase and improves salinity tolerance in Arabidopsis by enabling cytosolic K^+ retention and Na^+ exclusion. Journal of Experimental Botany **70**, 6349–6361.

Tang B, Yin C, Liu Q. 2019. Characteristics of ammonium and nitrate fluxes along the roots of *Picea asperata*. Journal of Plant Nutrition **42**, 772–782.

Tegg RS, Melian L, Wilson CR, Shabala S. 2005. Plant cell growth and ion flux responses to the streptomycete phytotoxin thaxtomin A: calcium and hydrogen flux patterns revealed by the non-invasive MIFE technique. Plant & Cell Physiology **46**, 638–648.

Tyerman SD, Beilby M, Whittington J, Juswono U, Newman I, Shabala S. 2001. Oscillations in proton transport revealed from simultaneous measurements of net current and net proton fluxes from isolated root protoplasts: MIFE meets patch–clamp. Australian Journal of Plant Physiology **28**, 591–606.

Vega A, O'Brien JA, Gutiérrez RA. 2019. Nitrate and hormonal signaling crosstalk for plant growth and development. Current Opinion in Plant Biology **52**, 155–163.

Walia A, Waadt R, Jones AM. 2018. Genetically encoded biosensors in plants: pathways to discovery. Annual Review of Plant Biology **69**, 497–524.

Wang F, Chen ZH, Liu X, Colmer TD, Shabala L, Salih A, Zhou M, Shabala S. 2017. Revealing the roles of GORK channels and NADPH oxidase in acclimation to hypoxia in *Arabidopsis*. Journal of Experimental Botany **68**, 3191–3204.

Wang F, Chen Z-H, Liu X, Shabala L, Yu M, Zhou M, Salih A, Shabala S. 2019. The loss of RBOHD function modulates root adaptive responses to combined hypoxia and salinity stress in *Arabidopsis*. Environmental and Experimental Botany **158**, 125–135.

Wang H, Shabala L, Zhou M, Shabala S. 2018. Hydrogen peroxide-induced root Ca^{2+} and K^+ fluxes correlate with salt tolerance in cereals: towards the cell-based phenotyping. International Journal of Molecular Sciences **19**, 702.

Wany A, Kumari A, Gupta KJ. 2017. Nitric oxide is essential for the development of aerenchyma in wheat roots under hypoxic stress. Plant, Cell & Environment **40**, 3002–3017.

Weits DA, Kunkowska AB, Kamps NCW, et al. 2019. An apical hypoxic niche sets the pace of shoot meristem activity. Nature **569**, 714–717.

Wu H, Shabala L, Azzarello E, et al. 2018. Na^+ extrusion from the cytosol and tissue-specific Na^+ sequestration in roots confer differential salt stress tolerance between durum and bread wheat. Journal of Experimental Botany **69**, 3987–4001.

Wu H, Shabala L, Zhou M, Su N, Wu Q, Ul-Haq T, Zhu J, Mancuso S, Azzarello E, Shabala S. 2019. Root vacuolar Na^+ sequestration but not exclusion from uptake correlates with barley salt tolerance. The Plant Journal **100**, 55–67.

Yu M, Lamattina L, Spoel SH, Loake GJ. 2014. Nitric oxide function in plant biology: a redox cue in deconvolution. New Phytologist **202**, 1142–1156.

Zeng F, Shabala S, Maksimović JD, Maksimović V, Bonales-Alatorre E, Shabala L, Yu M, Zhang G, Živanović BD. 2018. Revealing mechanisms of salinity tissue tolerance in succulent halophytes: a case study for *Carpobrotus rossi*. Plant, Cell & Environment **41**, 2654–2667.

Zhang Y, Sa G, Zhang Y, et al. 2016. *Paxillus involutus*-facilitated Cd^{2+} influx through plasma membrane Ca^{2+}-permeable channels is stimulated by H$_2$O$_2$ and H$^+$-ATPase in ectomycorrhizal *Populus* × *canescens* under cadmium stress. Frontiers in Plant Science **7**, 1975.

Zhao N, Wang S, Ma X, Zhu H, Sa G, Sun J, Li N, Zhao C, Zhao R, Chen S. 2016. Extracellular ATP mediates cellular K$^+$/Na$^+$ homeostasis in two contrasting poplar species under NaCl stress. Trees **30**, 825–837.

Zhou T, Hua Y, Xu F. 2017. Involvement of reactive oxygen species and Ca^{2+} in the differential responses to low-boron in rapeseed genotypes. Plant and Soil **419**, 219–236.